INSTITUTE OF PHYSICS PUBLISHING SUPERCONDUCTOR SCIENCE AND TECHNOLOGY

Supercond. Sci. Technol. **19** (2006) 161–168 doi:10.1088/0953-2048/19/2/002

Microstructures of MgB_2/Fe tapes fabricated by an *in situ* powder-in-tube method using MgH_2 as a precursor powder

S Hata[1,5], T Yoshidome[1], H Sosiati[2,3], Y Tomokiyo[1], N Kuwano[3], A Matsumoto[4], H Kitaguchi[4] and H Kumakura[4]

[1] Department of Applied Sciences for Electronics and Materials, Kyushu University, Kasuga 816-8580, Japan
[2] Research Laboratory for High Voltage Electron Microscopy, Kyushu University, Fukuoka 812-8581, Japan
[3] Art, Science and Technology Centre for Cooperative Research, Kyushu University, Kasuga 816-8580, Japan
[4] National Institute for Materials Science, Tsukuba 305-0047, Japan

E-mail: hata@asem.kyushu-u.ac.jp

Received 8 November 2005, in final form 30 November 2005
Published 4 January 2006
Online at stacks.iop.org/SUST/19/161

Abstract

Microstructures of MgB_2/Fe tapes fabricated by an *in situ* powder-in-tube method using MgH_2 as a precursor powder have been studied by means of x-ray diffraction and analytical transmission electron microscopy combined with a focused ion beam microsampling technique. The overall microstructures in the tapes are characterized as densely crystallized MgB_2 areas with 10–200 nm grain size, uncrystallized areas mainly containing MgO and amorphous phases enriched with B, and a number of holes and cracks. The crystallized MgB_2 areas increase upon doping with SiC nanoparticles. Si and C atoms decomposed from SiC nanoparticles during heat treatment exhibit different spatial distributions: the Si atoms are inhomogeneously distributed, forming silicides such as Mg_2Si with grain size of 5–20 nm, while the C atoms tend to be uniformly distributed in the MgB_2 matrix. A significant difference in distribution of O atoms between the SiC-doped and non-doped specimens was observed. The processes of formation of these microstructures and their relationships with the critical current density under magnetic fields have been discussed.

1. Introduction

Extensive research efforts as regards superconducting tapes of MgB_2 [1] are being made worldwide, intending to increase the critical current density (J_c). The J_c of *in situ* processed MgB_2 tapes depends sensitively on fabrication parameters, such as heat treatment conditions, starting materials and additional dopants. Since these parameters strongly influence the microstructures as well as the J_c properties of the *in situ* processed MgB_2 tapes, microstructural analysis helps one to understand the relationships between the fabrication parameters and the J_c properties.

This paper focuses on MgB_2/Fe tapes fabricated by an *in situ* powder-in-tube (PIT) method using MgH_2 as a precursor powder [2–6]. It has been reported that use of the MgH_2 powder in the *in situ* PIT process has a number of advantages over use of conventional Mg powder. Firstly, J_c values of MgB_2 tapes prepared with the MgH_2 powder are approximately double the values for those prepared with the Mg powder. Secondly, heat treatment temperatures can

[5] Author to whom any correspondence should be addressed.

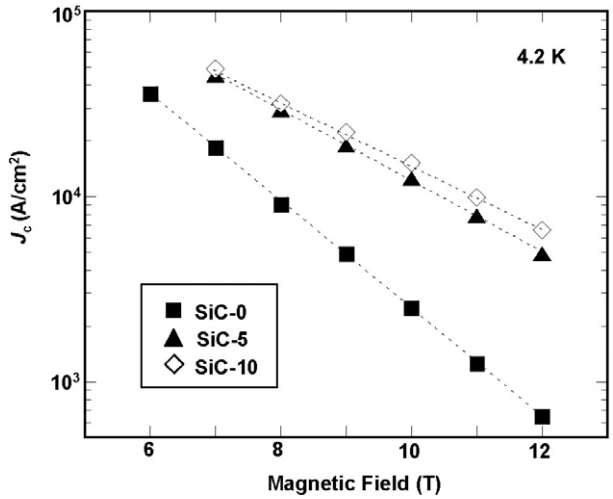

Figure 1. J_c for SiC-0, SiC-5 and SiC-10 as a function of the magnetic field.

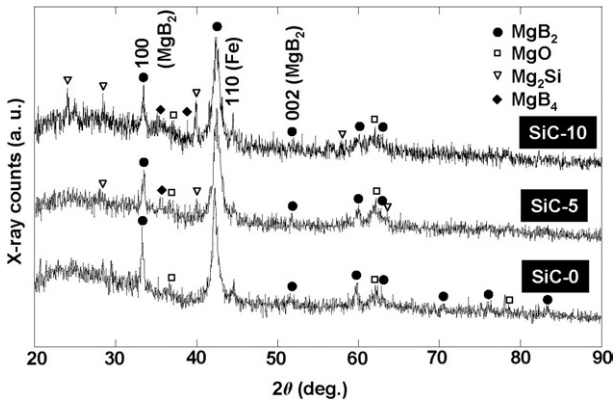

Figure 2. XRD patterns for SiC-0, SiC-5 and SiC-10.

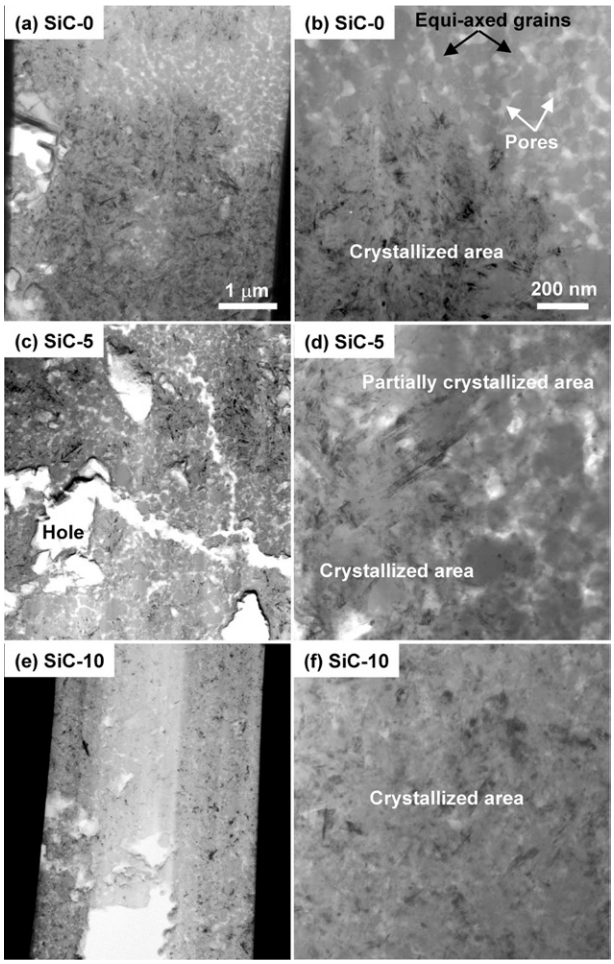

Figure 3. Low- and medium-magnification BF TEM images of SiC-0 ((a), (b)), SiC-5 ((c), (d)) and SiC-10 ((e), (f)).

be reduced without degrading the J_c values. Doping with impurities such as nanosized SiC [7–11] is also effective for enhancing J_c under magnetic fields [3–5]. Owing to these advantages, knowledge of microstructures of the MgB_2/Fe tapes prepared with the MgH_2 powder will be a good guide for developing MgB_2 tapes with excellent J_c properties. However, no detailed microstructural study of these tapes has been reported.

In the present study, microstructures of the MgB_2/Fe tapes fabricated by an *in situ* PIT method using MgH_2 as a precursor powder have been investigated in detail by means of x-ray diffraction (XRD) and analytical transmission electron microscopy (ATEM). Since microstructures in MgB_2 tapes and wires are often spatially inhomogeneous [12–15], a focused ion beam (FIB) microsampling technique [16] has been applied for specimen preparation. This technique can be used to prepare TEM specimens from desired areas in the MgB_2 tapes, which is beneficial for correctly characterizing microstructures over the entire area of the tapes. To the best of our knowledge, no other research groups have used this technique effectively for addressing MgB_2 tapes. Nanometre-scale elemental mapping using characteristic x-rays has also been carried out to clarify the two-dimensional (2D) distribution of constituent elements in the microstructures. On the basis of the results obtained, the formation of microstructure in the *in situ* PIT process and relationships between the microstructures and J_c properties will be discussed.

2. Experiment

The detailed procedure for preparation of MgB_2/Fe tapes using MgH_2 as a precursor powder has been reported elsewhere [2–5]. MgH_2 powder (325 mesh, 90%) and amorphous B powder (325 mesh, 99.9%) were mixed with the nominal composition ratio, Mg:B = 1:2. 5 or 10 at.% of SiC powders about 30 nm in size were doped into the mixed powder of MgH_2 and amorphous B. In this paper, the specimens of non-doped MgB_2 tape and SiC-doped MgB_2 tapes with 5 and 10 at.% SiC are designated as SiC-0, SiC-5 and SiC-10, respectively. These mixed powders were packed into pure Fe tubes 5 cm in length, and then cold-rolled into tapes. The final size of the tapes was about 4.5 mm width and 0.5 mm thickness. The tape specimens were heated under an Ar atmosphere up to 873 K for 0.5 h and kept at this temperature for 1 h, and then cooled in a furnace.

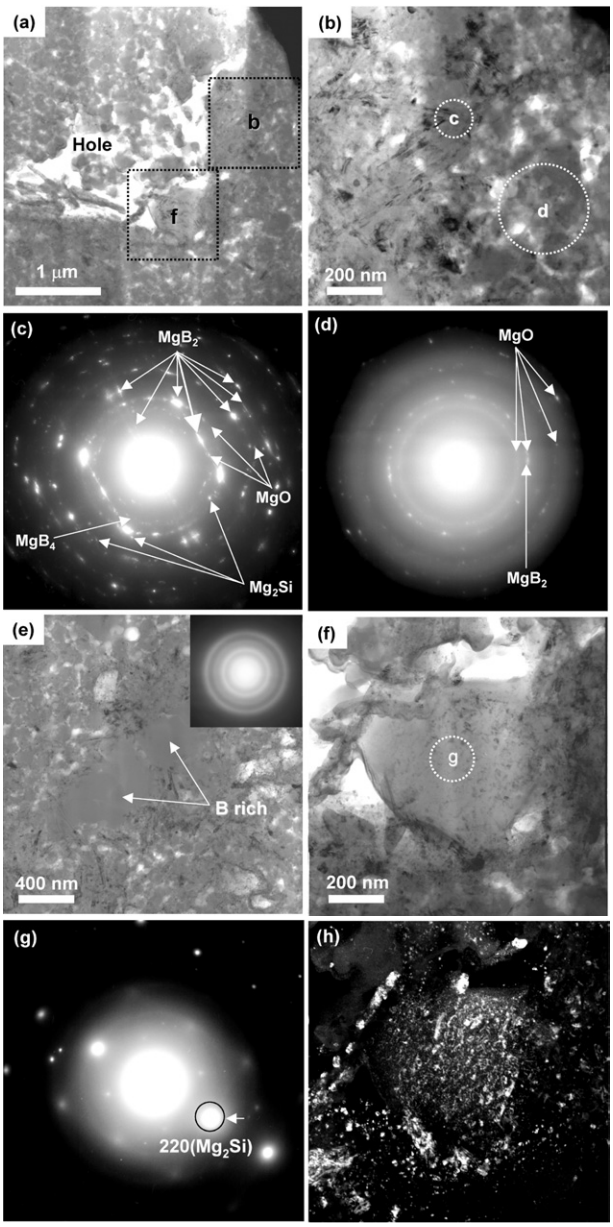

Figure 4. TEM results for SiC-5. (a) Low-magnification BF image; (b) enlarged image of area b in (a); (c) ED pattern taken from the encircled areas c and d in (b); (d) ED pattern taken from the encircled area d in (b); (e) BF image and an ED pattern of amorphous B-rich areas, (f) BF image of a large grain of Mg_2Si taken from area f in (a); (g) ED pattern of area g in (f); and (h) DF image obtained using the 220_{Mg_2Si} reflection in (g).

The critical current (I_c) of the tape specimens was measured by a four-probe resistive method in a magnetic field at 4.2 K. J_c was obtained by dividing the measured I_c by the cross-sectional area of the MgB_2 core. The criterion of 1 μV cm^{-1} was used for I_c determination. The magnetic field was applied parallel to the tape surface.

Crystalline phases in all specimens were identified from x-ray diffraction (XRD) results. Specimens for the XRD experiment were prepared by mechanically peeling off the MgB_2 core from the tape specimens. An FIB system (HITACHI FB-2000K) equipped with a microsampling unit was used for preparing TEM specimens. Microsamples with the size of 15 μm × 3 μm × 15 μm were picked up from the middle and edge parts of the MgB_2 core. A TEM (FEI TECNAI-F20) equipped with scanning TEM and energy dispersive x-ray spectroscopy (STEM-EDXS) systems was used for microstructural analysis. In the STEM-EDXS experiments, an electron beam about 1 nm in diameter was positioned on the specimen surface, and an EDX spectrum was acquired for 4 s at each position. Elemental maps were obtained by displaying integrated intensities of characteristic x-rays (B K: 0.18 keV, C K: 0.28 keV, O K: 0.53 keV, Mg K: 1.25 keV, Si K: 1.74 keV) at each of the acquisition points without background subtraction. All the specimens were cleaned with a plasma cleaner (ULVAC PLASMA CUBE C50-MK) before the STEM-EDXS experiments were carried out to prevent hydrocarbon contamination.

Table 1. Lattice parameters of MgB_2 determined from the XRD experiment in figure 2.

Specimen	a_{MgB_2} (nm)	c_{MgB_2} (nm)
SiC-0	0.3089	0.3533
SiC-5	0.3083	0.3532
SiC-10	0.3079	0.3533

3. Results

3.1. J_c properties

Figure 1 shows J_c for SiC-0, SiC-5 and SiC-10 as a function of the magnetic field. In magnetic fields up to 12 T, the J_c values for SiC-5 and SiC-10 are an order of magnitude higher than that for SiC-0. At the same magnitude of the magnetic field, J_c for SiC-10 is slightly higher than that for SiC-5. This clearly shows that the addition of nanosized SiC in the MgB_2 tapes has induced a marked enhancement of J_c, whereas an SiC doping level higher than 5 at.% yielded less pronounced effects on J_c.

3.2. XRD analysis

The XRD patterns of SiC-0, SiC-5 and SiC-10 in figure 2 show MgB_2 as a main phase and MgO, MgB_4 and Mg_2Si as impurity phases. The diffraction peaks from Fe seen in all the diffraction patterns are due to mixing of the Fe sheath material in the specimen preparation. No diffraction peak from SiC was identified, which suggests that the nanosized SiC was decomposed during the heat treatment. These XRD patterns also indicate that the Bragg angles of the reflections from MgB_2 slightly change with the SiC doping. The lattice parameters, a and c, of the hexagonal MgB_2 crystal were calculated from these Bragg angles, and these are shown in table 1. It is noted that the lattice parameter, a, decreases with increasing SiC content. This suggests that some of the B atoms in the MgB_2 crystal have been replaced with C atoms decomposed from the SiC nanoparticles [7, 9–11, 17, 18].

3.3. TEM analysis

Figures 3(a), (c) and (e) show bright-field (BF) TEM images of microsamples of SiC-0, SiC-5 and SiC-10, respectively.

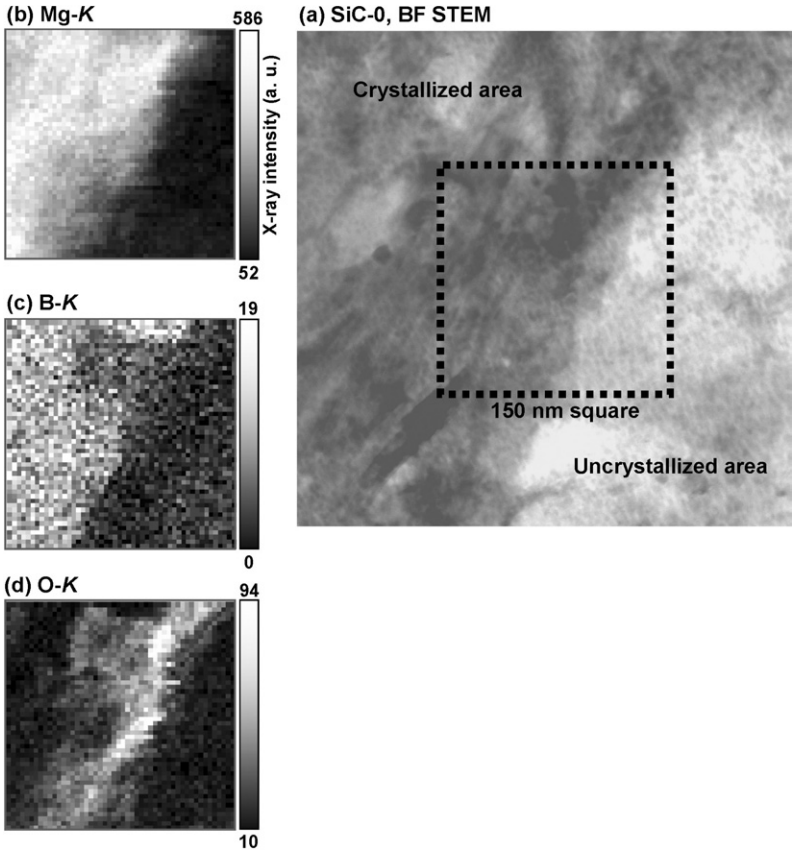

Figure 5. STEM-EDXS elemental mapping for SiC-0. (a) BF STEM image; (b) Mg K map; (c) B K map; and (d) O K map.

These microsamples were prepared from the middle of the MgB_2 core. All the specimens contain a number of holes and cracks, as reported by other researchers [12, 13]. Scanning electron microscopy observations confirmed that these holes and cracks were originally formed in the *in situ* PIT process. A magnified image of SiC-0 in figure 3(b) shows two different microstructures. One microstructure in the lower part of the image exhibits dark contrast due to diffraction in the crystals. Another microstructure in the upper part is composed of equi-axed grains with grey contrast and small pores with bright contrast, and similar microstructures have been observed by Li *et al* [19]. As described in detail later, the former microstructure corresponds to crystallized MgB_2 areas, and the latter corresponds to uncrystallized areas that mainly contain MgO and amorphous phases with B-rich compositions. The dark diffraction contrast in the crystallized areas shows that some of the MgB_2 crystals have needle-like shapes. This morphology of the MgB_2 crystals is a feature of the MgB_2 tapes prepared with the MgH_2 powder, as reported previously [3]. Figure 3(d) shows a magnified image of SiC-5. Dark diffraction contrast that suggests the crystallization of MgB_2 is observed in some of the uncrystallized areas. In the case of SiC-10 in figure 3(f), the crystallized areas have significantly increased, resulting in a homogeneous microstructure in the MgB_2 core. The grain size of MgB_2 is about 10–200 nm and not clearly dependent upon the SiC content.

Figure 4 shows the result of detailed TEM observation for SiC-5, as a representative of the three specimens: SiC-0, SiC-5 and SiC-10. A low-magnification BF image in figure 4(a) shows the inhomogeneous microstructure at the sub-μm scale as described above. A magnified image, figure 4(b), of the area b in figure 4(a) shows a mixture of crystallized and uncrystallized areas. An electron diffraction (ED) pattern, figure 4(c), taken from the encircled area c in figure 4(b) implies that the crystallized area contains MgB_2 as the main phase and MgO, Mg_2Si and MgB_4 as impurity phases. This agrees with the XRD result shown in figure 2. Since diffraction intensities from these crystalline phases appear very close to each other in the ED pattern, dark-field (DF) imaging of each of these phases is difficult. However, it is noted that some of the diffraction spots from MgB_2, for example, $hkl = 100_{MgB_2}$ indicated by the extra large arrow in figure 4(c), exhibit streaks. This indicates that the needle-shaped grains observed in the crystallized areas are of MgB_2. An ED pattern, figure 4(d), from the encircled area d in figure 4(b) shows the existence of MgO and amorphous phases with a small amount of MgB_2 in the uncrystallized area. EDXS experiments revealed that these uncrystallized areas have higher B and lower Mg concentrations than those in the crystallized areas. Therefore, it turns out that the amorphous phase is enriched with B. As a matter of fact, large grains of the amorphous B were recognized in the uncrystallized areas, as shown in figure 4(e). A magnified image, figure 4(f) of the area f in figure 4(a) shows a large grain of Mg_2Si about 500 nm in size, which was clearly identified from the ED pattern and the DF image in figures 4(g)

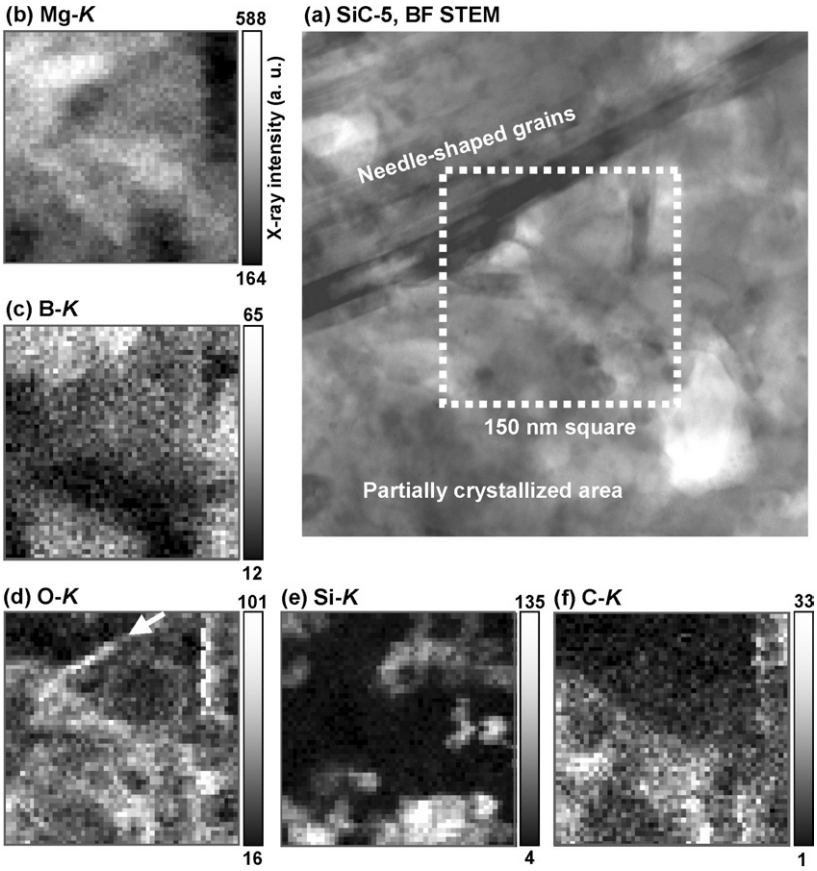

Figure 6. STEM-EDXS elemental mapping for SiC-5. (a) BF STEM image; (b) Mg K map; (c) B K map; (d) O K map; (e) Si K map; and (f) C K map.

and (h), respectively. No diffraction intensities relating to carbon (e.g. graphite) or carbide phases were recognized.

3.4. STEM-EDXS analysis

Figure 5 shows a result from the STEM-EDXS elemental mapping for Si-0. The broken open square in the BF STEM image, figure 5(a), indicates a mapping area 150 nm, square, in size, which contains a boundary between crystallized and uncrystallized areas. Since the uncrystallized area has very low density, elemental mapping data do not give straightforward information on the compositions in the two different areas. For example, very low concentrations of Mg (figure 5(b)) and B (figure 5(c)) atoms in the uncrystallized area are mainly due to the very low density in this area. Nevertheless, it is clearly seen that the 2D distribution of the constituent elements is well correlated with the microstructures. The O map (figure 5(d)) clearly shows enrichment of O atoms along the boundary between the crystallized and uncrystallized areas. It was found from TEM observations that MgO was formed in this O-rich area.

Figure 6 shows an elemental mapping result for SiC-5. The mapping area contains a boundary between a crystallized area with needle-shaped grains of MgB_2 and a partially crystallized area without needle-shaped grains. The enrichment of O atoms at the boundary between the crystallized and uncrystallized areas is recognized, as indicated by the arrow in figure 6(d). However, this enrichment of O atoms is less remarkable than that in the non-doped specimen. Si (figure 6(e)) and C (figure 6(f)) atoms show different distributions. This demonstrates that most of the SiC nanoparticles decomposed during the *in situ* PIT process [3–11]. The decomposed Si atoms are well localized in small areas 5–50 nm in size. This local enrichment of Si atoms is the most significant among those for all the impurity atoms, O, Si and C. The distribution of C atoms (figure 6(f)) is similar to that of O atoms (figure 6(d)) and opposite to that of B atoms (figure 6(c)). This is interpreted as indicating the formation of oxides such as Mg(B, O) [20, 21] and BO_x [22] or substitution of O and C atoms for B atoms in the MgB_2 matrix [7, 9–11, 17, 18, 23, 24].

Figure 7 shows an elemental mapping result for SiC-10. The mapping area again contains a crystallized area with needle-shaped grains and a partially crystallized area. The local Si-rich areas with the size of 5–20 nm increase in number with the SiC content, as depicted with white lines in figure 7(e). These white lines showing the Si-rich areas are also drawn in the other figures for the phase identification described below. It should be noted that O atoms in figure 7(d) tend to be enriched close to the Si-rich areas. On the other hand, C atoms in figure 7(f) tend to disperse uniformly irrespective of the distribution of the other elements. This may mean the substitution of C atoms for B atoms in the MgB_2 crystals, as expected from the XRD experiment. In this elemental mapping

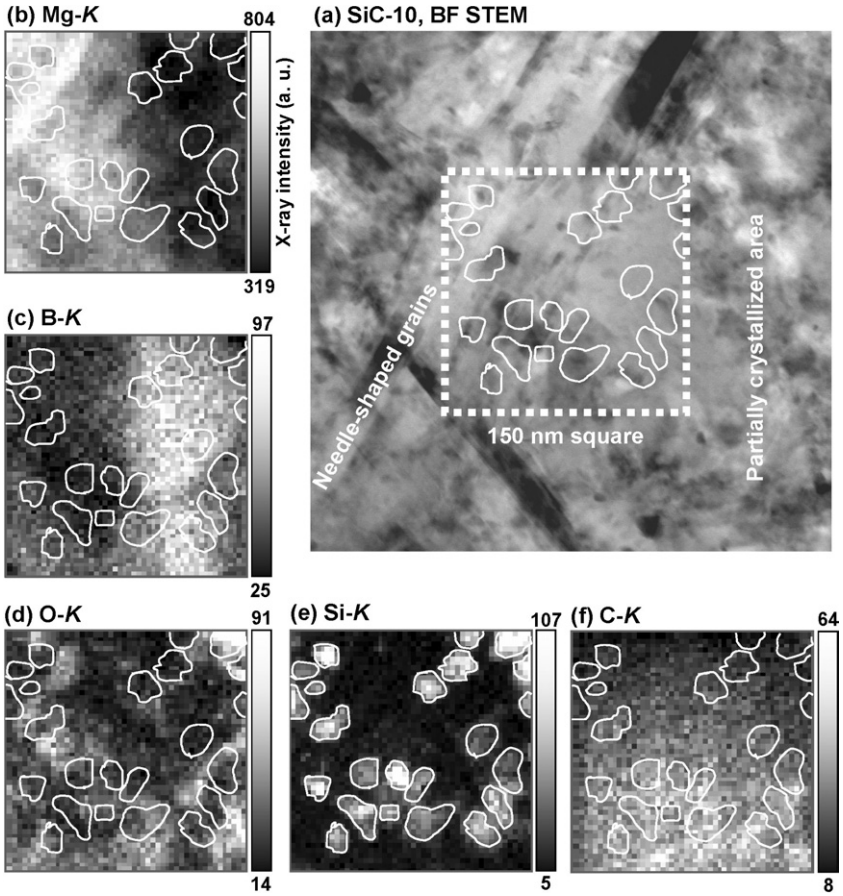

Figure 7. STEM-EDXS elemental mapping for SiC-10. (a) BF STEM image; (b) Mg K map; (c) B K map; (d) O K map; (e) Si K map; and (f) C K map.

for SiC-10, one can identify locations of some impurity phases by comparing the elemental maps with each other. For example, most of the Si-rich areas show lower Mg and lower O concentrations. These areas can be identified as Mg_2Si since the density of Mg atoms is lower in the Mg_2Si crystal (cubic CaF_2 type, $a = 0.6351$ nm) than in the MgB_2 crystal (hexagonal AlB_2 type, $a = 0.3086$ nm, $c = 0.3524$ nm). The other Si-rich areas where the above interpretation for Mg_2Si is not suitable may be nanosized silicides such as SiO_2 and $Si_xB_yO_z$ [10].

Figure 8 shows another elemental mapping result for SiC-10. The mapping area contains part of a large grain of Mg_2Si. Mg (figure 8(a)) and O (figure 8(d)) atoms are enriched at the peripheries of the Mg_2Si grain, suggesting the formation of MgO.

4. Discussion

4.1. Sample preparation by the FIB microsampling technique

It is emphasized that the FIB microsampling technique is effective for preparing TEM specimens of the present MgB_2/Fe tapes with inhomogeneous microstructures. The TEM observation combined with this technique revealed the existence of holes and cracks and the distribution of crystallized and uncrystallized areas at the sub-μm scale. As a result, influences of the nanosized SiC doping on these microstructures have been clearly observed. For a conventional TEM specimen preparation method using Ar ion milling, this kind of microstructure analysis is difficult since the uncrystallized areas with low density are preferentially milled and hardly any of the original inhomogeneous microstructure will remain.

4.2. Microstructure formation in an in situ PIT process

All the MgB_2/Fe tapes prepared with the MgH_2 powder show characteristic microstructures composed of crystallized MgB_2 areas and uncrystallized areas. The crystallized areas have compact granular structures of the MgB_2 crystals, which may be advantageous for increasing J_c [2–6]. The uncrystallized areas where the reaction for forming MgB_2 has not been completed are porous and mainly contain MgO and amorphous B-rich phases. In the case of the non-doped MgB_2/Fe tape, significant enrichment of oxygen due to the formation of MgO was observed along the boundary between the crystallized and uncrystallized areas. Since the present MgB_2/Fe tape specimens have been prepared using MgH_2 powder as a starting material, MgO may be produced in the air after the *in situ* PIT process. In other words, Mg-rich regions that would prevent crystallization of MgB_2 have been formed at the growth front of the crystallized areas in the non-doped MgB_2/Fe tape.

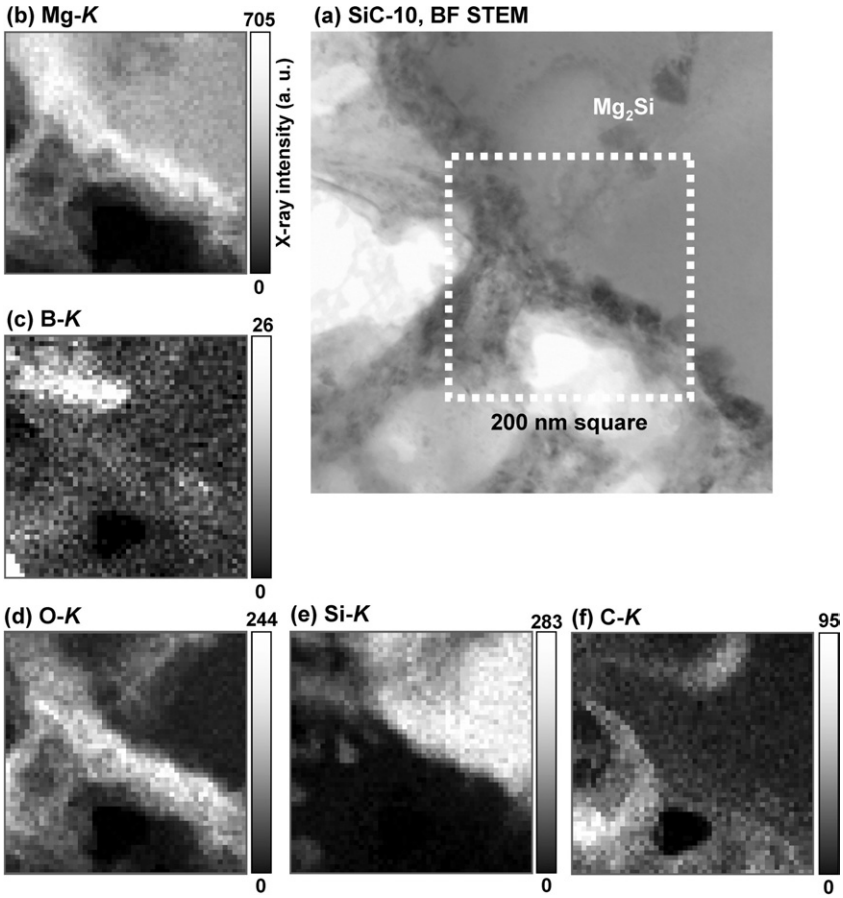

Figure 8. STEM-EDXS elemental mapping at a large grain of Mg_2Si in SiC-10. (a) BF STEM image; (b) Mg K map; (c) B K map; (d) O K map; (e) Si K map; and (f) C K map.

The crystallized area of MgB_2 in the tapes significantly increases with nanosized SiC doping. The boundaries between the crystallized and uncrystallized areas become ambiguous, and the preferential formation of MgO along the boundaries is suppressed. O atoms in the SiC-doped tapes tend to be uniformly distributed or enriched near Si-rich areas that are mainly of Mg_2Si. That is, the doping of SiC nanoparticles brings about changes in the distribution of O atoms in the MgB_2 tapes as well as the formation of nanosized silicides. A probable mechanism for the microstructure formation in the SiC-doped tapes would be as follows: in the early stages of the heat treatment that is described above, the SiC nanoparticles decompose into Si and C atoms; the decomposed Si atoms react with Mg atoms to form fine particles of Mg_2Si before starting the crystallization of MgB_2 [3, 5, 6]; the reaction for forming Mg_2Si consumes Mg atoms so the preferential enrichment of Mg atoms at the growth front of MgB_2 crystals can be suppressed. There is another possibility: that Mg-rich areas are formed around the Mg_2Si phase, as shown in figures 7 and 8, since the density of Mg atoms in the Mg_2Si phase is lower than that in the MgB_2 phase. Since these Mg-rich areas are small in size and dispersed with the nanosized Mg_2Si, their influences on the crystallization of MgB_2 will not be serious. As a result, the crystallization of MgB_2 proceeds well in the SiC-doped MgB_2 tapes. It is also expected that the fine Mg-rich areas in the SiC-doped tapes may be oxidized after the *in situ* PIT process and act as effective pinning centres. The decomposed C atoms, on the other hand, partly substitute for B atoms in the MgB_2 crystals, as supported by the XRD and STEM-EDXS data. This substitution behaviour enhances the upper critical field (B_{c2}) and contributes to the J_c increase under high magnetic fields [4].

4.3. Relationships between microstructures and J_c properties

As shown in figure 1, the present MgB_2/Fe tapes exhibit marked improvement of J_c under magnetic fields caused by the nanosized SiC doping. It is apparent that the improvement of J_c characteristics is correlated with the following microstructural changes with the SiC doping: (i) increase of the densely crystallized area of MgB_2; (ii) formation of nanosized silicides such as Mg_2Si; (iii) substantial dispersion of nanosized oxides such as MgO; and (iv) C substitution for B atoms in the MgB_2 crystals. The microstructural change (i) improves the flow of supercurrent, and (ii) and (iii) are well known to yield effective pinning centres for MgB_2 materials. The effect of (iv), from the SiC doping, has also been reported previously [4, 7, 10, 11]. These microstructural changes are more pronounced for SiC-10 than for SiC-5. However, the differences in J_c value between SiC-5 and SiC-10 are not so large, as shown in figure 1. Therefore, the excess doping of SiC nanoparticles is not the best way to effectively improve the J_c properties. A better way

to further improve J_c may be reducing the grain sizes of MgB_2 and impurity phases in order to increase the density of pinning centres such as grain boundaries and nanosized impurities, as shown in the microstructural study of MgB_2 films [25–30].

5. Summary

Microstructures of MgB_2/Fe tapes fabricated by an *in situ* PIT method using MgH_2 as a precursor powder have been investigated in detail. The results obtained are summarized as follows.

5 or 10 at.% doping of nanosized SiC in the MgB_2/Fe tape results in significant enhancement of J_c: for example, from 6×10^2 A cm^{-2} at 4.2 K and 12 T for the non-doped tape to 5×10^3 A cm^{-2} for the 5 at.% SiC-doped one.

By using the FIB microsampling technique for TEM specimen preparation, the microstructures of the MgB_2/Fe tapes are clearly characterized as densely crystallized MgB_2 areas with 10–200 nm grain size, uncrystallized areas mainly containing MgO and amorphous B-rich phases, and a number of holes and cracks. The nanosized SiC doping increases the crystallized areas and leads to the formation of homogeneous granular structures of MgB_2.

STEM-EDXS elemental mapping revealed the enrichment of O atoms due to the formation of MgO at the boundaries between the crystallized and uncrystallized areas. This enrichment of O atoms at the boundary areas is suppressed by SiC doping. O-rich areas in the SiC-doped MgB_2/Fe tapes are small in size and tend to be dispersed near Si-rich areas.

The increase of the densely crystallized area of MgB_2 improves the flow of supercurrent, and the formation of silicides, mainly Mg_2Si, with grain sizes of about 5–20 nm and the substantial dispersion of nanosized oxides such as MgO will raise the density of effective pinning centres. C substitution for B atoms in the MgB_2 crystals is supported by XRD and STEM-EDXS data for the SiC-doped specimens. These microstructural changes with SiC doping result in a marked improvement of J_c under magnetic fields.

Acknowledgments

This work was supported in part by Nanotechnology Support Project of the Ministry of Education, Culture, Sports, Science and Technology (MEXT), Japan and Research Promotion Bureau, MEXT, Japan under contracts No 16-556.

References

[1] Nagamatsu J, Nakagawa N, Muranaka T, Zenitani Y and Akimitsu J 2001 *Nature* **410** 63–4
[2] Fujii H, Togano K and Kumakura H 2002 *Supercond. Sci. Technol.* **15** 1571–6
[3] Matsumoto A, Kumakura H, Kitaguchi H and Hatakeyama H 2003 *Supercond. Sci. Technol.* **16** 926–30
[4] Kumakura H, Kitaguchi H, Matsumoto A and Hatakeyama H 2004 *Appl. Phys. Lett.* **84** 3669–71
[5] Matsumoto A, Kumakura H, Kitaguchi H and Hatakeyama H 2004 *Supercond. Sci. Technol.* **17** S319–23
[6] Jiang C H, Hatakeyama H and Kumakura H 2005 *Supercond. Sci. Technol.* **18** L17–22
[7] Dou S X, Soltanian S, Horvat J, Wang X L, Zhou S H, Ionescu M, Liu H K, Munroe P and Tomsic M 2002 *Appl. Phys. Lett.* **81** 3419–21
[8] Wang X L, Yao Q W, Horvat J, Qin M J and Dou S X 2004 *Supercond. Sci. Technol.* **17** L21–4
[9] Wang X L, Soltanian S, James M, Qin M J, Horvat J, Yao Q W, Liu H K and Dou S X 2004 *Physica* C **408–410** 63–7
[10] Dou S X, Braccini V, Soltanian S, Klie R, Zhu Y, Li S, Wang X L and Larbalestier D 2004 *J. Appl. Phys.* **96** 7549–55
[11] Soltanian S, Wang X L, Hovart J, Dou S X, Sumption M D, Bhatia M, Collings E W, Monroe P and Tomsic M 2005 *Supercond. Sci. Technol.* **18** 658–66
[12] Serquis A *et al* 2002 *J. Appl. Phys.* **92** 351–6
[13] Serquis A, Civale L, Hammon D L, Liao X Z, Coulter J Y, Zhu Y T, Peterson D E and Mueller F M 2003 *J. Appl. Phys.* **94** 4024–31
[14] Eyidi D, Eibl O, Wenzel T, Nickel K G, Giovannini M and Saccone A 2003 *Micron* **34** 85–96
[15] Eyidi D, Eibl O, Wenzel T, Nickel K G, Schlachter S I and Goldacker W 2003 *Supercond. Sci. Technol.* **16** 778–88
[16] Ishitani T, Umemura K, Ohnishi T, Yaguchi T and Kamino T 2004 *J. Electron Microsc.* **53** 443–9
[17] Dou S X, Yeoh W K, Horvat J and Ionescu M 2003 *Appl. Phys. Lett.* **83** 4996–8
[18] Cava R J, Zandbergen H W and Inumaru K 2003 *Physica* C **385** 8–15
[19] Li S, Prabhakar O, Tan T T, Sun C Q, Wang X L, Soltanian S, Horvat J and Dou S X 2002 *Appl. Phys. Lett.* **81** 874–6
[20] Liao X Z, Serquis A C, Zhu Y T, Huang J Y, Peterson D E, Mueller F M and Xu H F 2002 *Appl. Phys. Lett.* **80** 4398–400
[21] Liao X Z, Serquis A, Zhu Y T, Huang J Y, Civale L, Peterson D E and Mueller F M 2003 *J. Appl. Phys.* **93** 6208–15
[22] Klie R F, Idrobo J C, Browning N D, Regan K A, Rogado N S and Cava R J 2001 *Appl. Phys. Lett.* **79** 1837–9
[23] Klie R F, Idrobo J C, Browning N D, Serquis A, Zhu Y T, Liao X Z and Mueller F M 2002 *Appl. Phys. Lett.* **80** 3970–2
[24] Klie R F and Zhu Y 2005 *Micron* **36** 219–31
[25] Sosiati H, Hata S, Kuwano N, Tomokiyo Y, Matsumoto A, Fukutomi M, Kitaguchi H, Komori K and Kumakura H 2004 *Physica* C **412–414** 1376–82
[26] Hata S, Sosiati H, Tomokiyo Y, Kuwano N, Matsumoto A, Fukutomi M, Kitaguchi H, Komori K and Kumakura H 2004 *J. Japan Inst. Metals* **68** 648–55
[27] Hata S, Sosiati H, Kuwano N, Tomokiyo Y, Matsumoto A, Fukutomi M, Kitaguchi H, Komori K and Kumakura H 2005 *IEEE Trans. Appl. Supercond.* **15** 3238–41
[28] Kitaguchi H, Matsumoto A, Kumakura H, Doi T, Yamamoto H, Saitoh K, Sosiati H and Hata S 2004 *Appl. Phys. Lett.* **85** 2842–4
[29] Kitaguchi H, Doi T, Kobayashi Y, Matsumoto A, Sosiati H, Hata S, Fukutomi M and Kumakura H 2005 *IEEE Trans. Appl. Supercond.* **15** 3313–6
[30] Sosiati H *et al* 2005 *Supercond. Sci. Technol.* **18** 1275–9